Fluence distribution of terrestrial gamma ray flashes observed by the Fermi Gamma-ray Burst Monitor

D. Tierney,[1] M. S. Briggs,[2,3] G. Fitzpatrick,[1] V. L. Chaplin,[2] S. Foley,[1] S. McBreen,[1] V. Connaughton,[2,3] S. Xiong,[2] D. Byrne,[1] M. Carr,[1] P. N. Bhat,[2] G. J. Fishman,[4] J. Greiner,[5] R. M. Kippen,[6] C. A. Meegan,[7] W. S. Paciesas,[7] R. D. Preece,[2,3] A. von Kienlin,[5] and C. Wilson-Hodge[8]

Received 11 July 2013; revised 9 September 2013; accepted 17 September 2013.

[1] The observed γ ray fluence distribution of terrestrial gamma ray flashes (TGFs) detected by the Fermi Gamma-ray Burst Monitor (GBM) is altered by instrumental effects. We perform corrections for dead time, pulse pileup, and detection efficiency in a model-independent manner. A sample of 106 GBM TGFs is selected to include both TGFs that triggered GBM and weaker TGFs found using an off-line search. Detector dead time and pulse pileup lower the observed fluence of each TGF and the detection efficiency causes weaker TGFs to have a lower probability of detection than brighter TGFs. Monte Carlo simulations are performed in each case to correct for these effects. The corrected fluence distribution is well fit with a power law of index $\alpha = -2.20 \pm 0.13$. This is consistent with previous estimates using other techniques. Neither a high-fluence cutoff nor a low-fluence limit is found. The fluence distribution is also expressed in units of TGF h^{-1} km^{-2} versus photons cm^{-2} per TGF.

Citation: Tierney, D., et al. (2013), Fluence distribution of terrestrial gamma ray flashes observed by the Fermi Gamma-ray Burst Monitor, *J. Geophys. Res. Space Physics*, *118*, doi:10.1002/jgra.50580.

1. Introduction

[2] Terrestrial gamma ray flashes (TGFs) are produced in a short intense flash with duration (T_{90}) of $\approx$ 250 μs [e.g., *Gjesteland et al.*, 2010; *Briggs et al.*, 2013]. The temporal profiles of these events consist of one or sometimes several pulses, each of which can generally be fit with a Gaussian or lognormal function [*Briggs et al.*, 2010; Foley et al., Pulse properties of terrestrial gamma-ray flashes detected by the Fermi Gamma-ray Burst Monitor, *Astrophysical Journal*, in preparation, 2013]. A review of observational and theoretical work in TGFs is presented in *Dwyer et al.* [2012] and references therein.

[3] Observations of TGFs generally come from γ ray instruments on satellites that have other prime scientific objectives. TGFs were first discovered by *Fishman et al.* [1994] by analyzing data from the Burst and Transient Source Experiment on the Compton Gamma Ray Observatory. Since then, TGFs have also been observed and studied by several other space-based γ ray instruments including the Reuven Ramaty High Energy Solar Spectroscopic Imager (RHESSI) [*Grefenstette et al.*, 2009; *Gjesteland et al.*, 2012], the Astro-rivelatore Gamma a Immagini Leggero [*Marisaldi*, 2011], and both the Large Area Telescope (LAT) [*Grove et al.*, 2012] and the Gamma-ray Burst Monitor (GBM) [*Fishman et al.*, 2011; *Briggs et al.*, 2013] on board the Fermi Gamma-ray Space Telescope.

[4] Each instrument observes a sample of TGFs which depends on several factors, such as sensitivity, energy range, and orbit. Many physical variables such as TGF-satellite distance, TGF altitude, TGF beaming angle, and intrinsic strength are convolved in the observed distribution. Recent work has connected the properties of the observed distribution with the source distribution of TGFs [*Carlson et al.*, 2012].

[5] One key question concerns the total number of TGFs/km^2/yr and the fluence distribution of these TGFs. *Collier et al.* [2011] suggest that the observed TGF counts distribution may take the form of a power law with more intense events being observed less frequently. *Østgaard et al.* [2012] go further to attempt to calculate the true distribution of TGF fluences by comparing the relative sensitivities and relative detection rate of RHESSI and GBM. Using this technique and assuming a power law distribution, an index of -2.3 ± 0.2 is estimated. A dead-time-corrected distribution of RHESSI TGFS was also fit by *Østgaard et al.* [2012] with a power law of index ranging between –2.3 and –3.0, depending on the binning.

[1]School of Physics, University College Dublin, Dublin, Ireland.
[2]CSPAR, University of Alabama in Huntsville, Huntsville, Alabama, USA.
[3]Department of Physics, University of Alabama in Huntsville, Huntsville, Alabama, USA.
[4]Jacobs Engineering Inc., Huntsville, Alabama, USA.
[5]Max-Planck-Institut für extraterrestrische Physik, Garching, Germany.
[6]Los Alamos National Laboratory, Los Alamos, New Mexico, USA.
[7]Universities Space Research Association, Huntsville, Alabama, USA.
[8]Space Science Office, NASA Marshall Space Flight Center, Huntsville, Alabama, USA.

Corresponding author: D. Tierney, School of Physics, University College Dublin, Stillorgan Rd., Belfield, Dublin 4, Ireland. (david.tierney@ucd.ie)

2169-9380/13/10.1002/jgra.50580

[6] To determine the TGF fluence distribution, our sample is selected from the extended range of GBM TGFs in *Briggs et al.* [2013], which significantly increases the fluence range. We control the number of triggered TGFs (generally strong) in the sample and the number of TGFs found only with the ground search (generally weak) [*Briggs et al.*, 2013] so that the distribution is unbiased with respect to TGF fluence. We rigorously take into account instrumental effects of GBM for each TGF in this large uniform sample. Finally, we do not assume a model to obtain the fluence distribution which results in a model-independent fluence distribution.

2. The Gamma-Ray Burst Monitor

[7] The Fermi Gamma-ray Space Telescope was launched on 11 June 2008 and observes several energy decades from ∼8 keV to ∼300 GeV using two instruments. The primary Large Area Telescope (LAT) [*Atwood et al.*, 2009] is a pair production telescope operating between 20 MeV and 300 GeV and the secondary Gamma-ray Burst Monitor (GBM) [*Meegan et al.*, 2009] comprises 14 scintillators operating between 8 keV and 40 MeV. These 14 scintillators are further composed of 12 low-energy sodium iodide (NaI) scintillation detectors with an energy range of 8–1000 keV and two high-energy bismuth germanate (BGO) scintillation detectors operating in the energy range of ∼ 200 keV to ∼ 40 MeV. The BGO detectors were primarily used in this analysis because they suffer less from instrumental effects compared to the NaI detectors. The NaI detectors have a role in the sample since their signal is used to detect TGFs; this is included in the evaluation of the detection efficiency.

2.1. Instrumental Effects

[8] It should be noted that GBM is not optimized for the study of TGFs, and instrumental factors such as dead time, pulse pileup, and detection efficiency must be taken into account to estimate the true number of counts observed by an ideal detector. As all instrumental effects can distort the observed properties of a TGF, it is necessary to define regimes where the effects are significant and to correct for these effects.

2.1.1. Dead Time

[9] For two counts (a count is a photon or a particle) to be recorded as individual events, the counts must be separated by a minimum amount of time. When a high-energy photon/particle interacts in one of the GBM BGO detectors, it creates optical photons that are then converted into an electrical signal by photomultiplier tubes. If this signal exceeds a certain threshold, it is sent to a specialized firmware to identify the peak. The signal is sampled at 9.6 MHz (∼ every 104 ns) and the firmware identifies the peak after four successive lower samples past the peak. The next 21 samples are ignored to allow the electronics to restabilize, thus giving the dead time of 2.6 μs after the peak [e.g., *Meegan et al.*, 2009; *Briggs et al.*, 2010; *Chaplin et al.*, 2013]. If the peak of the signal is recorded in the overflow channel (≃ 40 MeV in the BGO detectors), a larger dead time of ∼10 μs is initiated.

[10] A typical TGF is observed in the BGO detectors with a peak count rate of ∼100 kilocounts per second (kcps). This corresponds to a count rate of 1 count every ≈10 μs. The effects of GBM dead time on this observed count rate are nonnegligible because the count rate is of the order of the dead time (nominally 2.6 μs). The true rate is estimated via an iterative model-dependent deconvolution method which determines the most likely solution with uncertainties determined by Poisson uncertainties (section 4.2). The largest cause of unobserved photons in GBM is simple dead time which is nonparalyzable, but there are additional minor paralyzable dead-time losses due to pulse pileup [*Chaplin et al.*, 2013].

2.1.2. Pulse Pileup

[11] Pulse pileup (PPU) can alter the temporal and spectral properties of a TGF and can be quantified in two ways: peak PPU and tail PPU. Peak PPU occurs when two (or more) events occur in the detector in close temporal proximity [*Chaplin et al.*, 2013]. The peak signal for the first event is identified and before it can be registered as a count, the second event causes the signal to increase again. This causes the two pulses to be indistinguishable from a single pulse and be recorded as a single count. As two interactions have taken place in the detector, the signal is initially detected at the first count but the dead time will not begin until the second count is processed. For this effect to occur, the detector must register events within ∼0.4 μs of each other.

[12] Tail PPU occurs when the electronic signal has not stabilized to the background level and is still negative after the dead time has elapsed [*Meegan et al.*, 2009, Figure 7] (Figure 1 of *Chaplin et al.* [2013] shows an analytic approximation of the pulse shape). If the detector observes an event in this time interval, it will either be placed in a lower channel or may not have enough energy to create a signal that can bring it up to the threshold where it would be identified by the pulse height analyzer. This count can be lost even though it would have exceeded the threshold. Both peak and tail PPU can cause paralyzable dead time and can intensify issues with the background stabilization in the signal-processing electronics.

2.1.3. TGF Detection Efficiency

[13] The probability that GBM TGF search software [*Briggs et al.*, 2013] detects a TGF with a certain set of parameters defines the detection efficiency. Although TGFs have a high peak count rate (∼ 10^5 counts/s), the short time scales (∼250 μs) mean that only tens of counts/BGO/TGF are observed. The background noise, statistical variations in a TGF, instrumental effects, and TGF pulse properties determine at what efficiency a TGF with a given set of parameters can be detected. Weaker TGFs require the greatest detection efficiency correction due to the low signal-to-noise ratio and the larger percentage of statistical variability in the observed counts.

3. Sample Selection

[14] The TGFs in this study were selected based on the sample of TGFs in *Briggs et al.* [2013]. The TGFs were selected evenly over a calendar year to account for the seasonal variation in the global distribution of TGFs. During this time, GBM downloaded continuous photon counting data (i.e., time-tagged event (TTE) data) over three known active TGF regions (America, Africa, and Australia) to find weaker TGFs. The sample selection was biased to the American region where data were downloaded for about twice as long as any other region. Multiple triggering

algorithms were used on board to detect TGFs during this time and did not vary over the range of the sample (last modified on 10 November 2009 [*Fishman et al.*, 2011]). It should be noted that due to hardware limitations, the shortest timescale for onboard triggering is 16 ms, which greatly exceeds the typical TGF duration.

[15] TGFs detected between September 2010 and August 2011 both by onboard triggering and by ground search of the continuous TTE data were used. A stronger probability cut ($P_{\text{joint}}^{\text{corr}} < 10^{-16}$) was invoked than by *Briggs et al.* [2013] to ensure all TGFs have sufficient statistics to perform the analysis. Terrestrial electron beams were also removed from the sample. After these cuts, the sample comprised 37 triggered TGFs and 290 nontriggered TGFs.

[16] Approximately one third of this sample, 12 triggered and 94 ground-search TGFs, was selected for analysis. Due to the intense computational requirements, the entire sample could not be simulated; however, this sample was selected as a representative subsample. The same fraction of TGFs were selected from each sample (triggered and nontriggered) to avoid differently scaling the samples in later analysis. Several criteria such as location, chance probability of occurrence, cosmic ray filters, and observation by Fermi LAT were used to ensure only TGFs remain in the sample [*Briggs et al.*, 2013].

4. Method

[17] The temporal (counts) profile of a TGF observed by the GBM BGO detectors must be corrected for instrumental effects if an accurate fluence distribution is to be obtained. Several major effects are taken into account in this work: (1) a statistical deconvolution to correct for ordinary dead time (i.e., 2.6 μs per count), (2) simulations to quantify and correct for additional dead time from both peak and tail PPU, and (3) a correction for the detection efficiency.

4.1. TGF Pulse Fitting Process

[18] To determine satisfactory initial parameters for the dead-time deconvolution, a TGF pulse fit was performed to the counts profile of each TGF in the BGO detectors. Most time profiles were fit with single pulses; a few with two pulses (see section 5). Two pulse types, a Gaussian and a lognormal, were fit. More complex models were not fit as there were not enough counts per TGF to constrain additional model parameters. The Poisson likelihood for each fit was compared using the Akaike Information Criterion (AIC) [*Akaike*, 1974] to determine whether it was necessary to select the lognormal model over the Gaussian model. To select a lognormal function as a better fit over a Gaussian function, the difference in AIC was selected to be greater than 3 [*Burnham*, 2002]. More details on the TGF pulse fitting method can be found in Foley et al. (in preparation, 2013).

4.2. Dead-Time Deconvolution Process

[19] The dead-time deconvolution process simulated an input count profile as a nonhomogeneous Poisson process over the entire duration ($\gg T_{90}$) of a TGF [*Lewis and Shedler*, 1978] and then applies a dead-time filter to this profile [*Briggs et al.*, 2010]. The resulting filtered counts profile was compared to the TGF TTE data and a likelihood value is determined. This process was then repeated until the most likely solution was determined. The BGO detectors were used to limit issues with counts in the overflow spectral bin where a longer dead time was applied. The NaI detectors could not be used due to the high fraction of overflow counts/detector/TGF. There was no spectral dependence on the deconvolution process. The data can be binned in time for display purposes but the fitting was done using individual counts at the full resolution of the data (2 μs).

[20] The initial TGF pulse type and parameters were defined by the user. The TGF pulse was simulated by creating a stationary Poisson process determined by the maximum count rate of the simulated TGF and then filtered according to the shape of the pulse. A background was simulated using a stationary Poisson process determined from the local background rate of the TGF TTE data. Both sets of simulated data were then combined to determine the model for the predead-time-filtered counts profile.

[21] The simulated TGF pulse was then filtered to simulate the dead time of the GBM instrument. This process began at the first count and continued through the data set on a count by count basis. As there is high Poisson variability in TGFs with a low total number of counts, the simulation and filtering process was performed 2×10^6 times. The 2×10^6 simulations were then combined and divided by the total number of simulations. The average postfiltered TGF pulse was then compared to the input data and the likelihood for these parameters was determined. The parameters were then varied using the Nelder-Mead method [*Nelder and Mead*, 1965] and this procedure was repeated until a solution of maximum likelihood was determined. Only standard dead time was corrected; no attempt was made to account for overflow counts with longer dead time. Only three overflow counts occurred during the duration of a TGF in the whole sample and only one of these counts occurred where the average spacing between counts was less than 10 μs.

4.3. Pulse Pileup

[22] Software developed by *Chaplin et al.* [2013] was used to quantify the magnitude of the additional effects of PPU on TGFs observed by GBM. This software simulates the GBM electronics and filters an input counts profile (taking into account spectral properties) for peak and tail pulse pileup in combination with dead-time effects. To calculate the effects of PPU, simulated TGFs were filtered separately using this process and the dead-time-only filter. Each set of filtered data was then input into the dead-time deconvolution code to investigate how well the original simulated TGF pulse was recovered. A range of TGFs were simulated for this investigation, with peak rates between 50 and 500 kcps and three different input spectra, a low-energy range spectrum (0.15–1 MeV), a medium-energy range spectrum (1–10 MeV), and a broad-energy range spectrum (0.15–40 MeV).

4.4. Detection Efficiency of Observed TGFs

[23] Due to the low number of counts in a TGF, statistical variations can play a large role in determining whether or not a TGF is detected. The detection efficiency of TGFs observed by GBM was determined to correct the lower end of the fluence distribution and to determine the point at which TGFs are detected at 100% efficiency.

[24] A range of TGF parameters were simulated to observe how the detection efficiency varied as a function of these parameters. Both BGO and NaI detectors were simulated as data from both detector types are used in the actual TGF detection [*Briggs et al.*, 2013]. BGO detectors were simulated by defining a temporal (counts) profile and a background of 2 kcps. The BGO background is quite stable with minor variations between 1.4 and 5.5 kcps (median of ∼1.8 kcps). The dead-time filter was then applied to the simulated BGO files. A study of the observed counts/TGF in the BGO detectors versus the observed counts/TGF in the NaI detectors showed that the counts/TGF in the NaI detectors were on average ∼ 1.6 times the observed counts/TGF in the BGO detectors. This result was used to simulate the number of counts in the NaI detectors with a representative background of 1.1 kcps per detector.

[25] The simulated TGFs were then analyzed using the GBM TTE ground-search software to check if the event would pass the event detection and TGF classification criteria [*Briggs et al.*, 2013]. The stricter probability defined in section 3 was taken as the minimum acceptance threshold probability. A range of physically motivated parameters were simulated for normal and lognormal pulses. A low peak rate was initially selected for a set of parameters and gradually increased until the detection efficiency reached 100%. This process was repeated for each set of input parameters and each set of input parameters was simulated 1000 times.

5. Results

[26] Of the 106 TGFs in this sample, 13 are best fit with lognormal pulses and 93 are best fit with Gaussian pulses. Only one triggered TGF is best fit with lognormal function. Out of the 12 triggered TGFs, three are multipulsed TGFs comprising two Gaussian pulses each. No ground-search (nontriggered) TGFs are multipulsed. Because ground-search TGFs have lower observed counts, multipulsed events with no separation between the pulses may be more difficult to resolve and if an event is multipulsed, it is more likely to trigger the instrument due to the higher accumulation of counts within the 16 ms trigger interval.

[27] The ratio of lognormals to Gaussians in this sample is lower than the ratio observed by Foley et al. (in preparation, 2013). Compared to Foley et al. (in preparation, 2013), which uses only bright TGFs and uses the summed counts in all the GBM detectors, our sample includes many faint TGFs and uses just the BGO detectors. The resulting fewer counts will frequently result in insufficient statistics for the AIC to prefer the lognormal function over a Gaussian. A likely cause of TGFs tails is Compton scattering, which results in a tail that is softer than the primary pulse [*Østgaard et al.*, 2008; *Grefenstette et al.*, 2008; *Celestin and Pasko*, 2012]. By using only the high-energy BGO detectors, our profiles are biased toward the primary TGF pulse and against softer tails, another reason that the lognormal function may not be selected by the AIC over the Gaussian function.

5.1. Deconvolution Method

[28] The dead-time deconvolution code has been tested using simulations involving the effects of dead time alone and also including effects from PPU. Tests were performed to determine how accurately the code could reconstruct simulated TGFs that had been dead-time filtered. The study was performed over a large range of TGF parameters extending from TGFs on the threshold of detection to extremely bright TGFs. All parameters were reconstructed within the uncertainties. The uncertainties in the reconstructed parameters were larger for lognormal TGFs which are attributed to the additional free model parameter.

[29] The major effects of applying the dead-time correction were on the maximum rate and total counts of the TGF pulse. Other temporal parameters such as the full width at half maximum (FWHM) and rise/fall times were not significantly affected by applying the correction as is shown in Figure 1 (see also Foley et al. (in preparation, 2013)).

5.2. PPU Correction

[30] The dead-time deconvolution method (section 4.2) is used to correct the observed TGF count fluence. This method corrects for the primary dead time of GBM, the 2.6 μs window after each count in which the electronics are disabled by design. We test for the additional dead time due to PPU by comparing simulated TGF data filtered using the dead-time-only filter and simulated data filtered using the PPU and dead-time filter from *Chaplin et al.* [2013]. The simulations show that there was no significant difference between the two filters up to a maximum input rate of ≈350 kcps. For maximum input rates between 350 and 500 kcps, the PPU filter resulted in 10% higher dead time than the regular dead-time filter. Since the analytical approximation of the bipolar pulse in *Chaplin et al.* [2013] over-weights the negative portion of the bipolar pulse compared to the positive portion, the estimated fraction of the additional dead time due to PPU may be slightly overestimated. This is a small effect as only seven TGFs in the sample have a deconvolved maximum rate in the range of 350–500 kcps (the highest rate in the sample was 470 kcps) and the dead-time-corrected fluence of these TGFs was multiplied by 1.1 to correct for additional dead time from PPU.

5.3. Detection Efficiency

[31] The detection efficiency is approximately proportional to the integrated area under the input TGF pulse per detector (i.e., the total number of corrected counts/BGO/TGF). The detection threshold is 4.9 ± 0.8 counts per BGO, above which the detection efficiency increases linearly to 11.8 ± 1.1 counts per BGO which is the 100% efficiency limit. Using this correction, the number of TGFs in the sample is corrected from 106 observed TGFs up to 161 corrected TGFs.

5.4. Corrected Fluence Distributions

[32] The measured fluence distribution is modified by instrumental effects: TGFs are observed as weaker overall because of the losses of counts from dead time and the detection efficiency causes fewer weak TGFs to be observed. The dead-time and PPU corrections have the effect of shifting TGFs to higher fluences. Detection efficiency multiplies the number of TGFs with a given fluence to account for the low detection probabilities for weaker TGFs. These instrumental corrections are applied to the observed fluence distribution to obtain the corrected fluence distribution (Figure 2). The lowest bin in the correct distribution is the only bin that needed

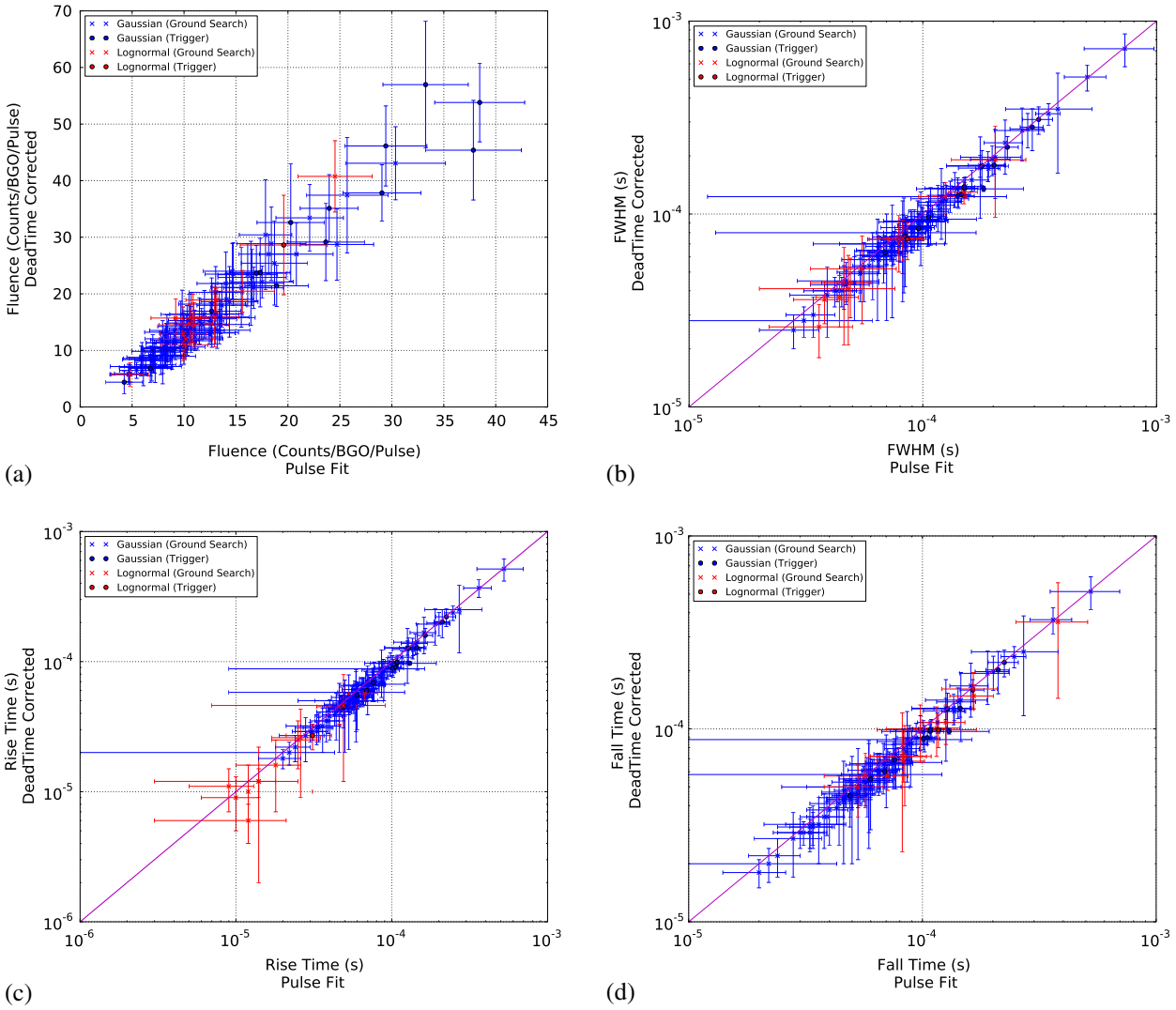

Figure 1. Dead-time-corrected parameters versus pulse fit parameters of 109 pulses from the 106 TGFs in the sample for (a) the fluence, (b) the full width at half maximum (FWHM),(c) the rise time, and (d) the fall time. A line of 45° is plotted to highlight the near 1:1 relationship between the temporal parameters before and after the dead-time correction is applied.

an increase because of detection efficiency (increase from 34 observed TGFs to 89 corrected TGFs).

[33] The corrected distribution is well fit with power law function with an index of –2.20 ± 0.13 and a normalization of 1640 ± 450 counts/BGO using an unbinned likelihood analysis. No high- or low-fluence cutoff is necessary. An exponential function was also fit to these data and gave a significantly worse fit. The detection efficiency effect manifests as a rollover in the raw fluence distribution below ∼ 10 counts/BGO/TGF, thus a power law is fit to the high-fluence tail of the raw distribution to obtain an index of –2.86 ± 0.32.

[34] Figure 2 has been scaled to show the photons observed as a function of effective area of the BGO detectors by assuming a single spectral model. In previous works [cf. *Briggs et al.*, 2010; *Østgaard et al.*, 2012], the effective area of the individual GBM BGO detectors was estimated from a graph of the effective area [*Meegan et al.*, 2009] as ∼160 cm^2. For five TGFs observed with varying spacecraft orientations and altitudes (average = 559 km), a power law with an exponential cutoff at 7.3 MeV [e.g., *Dwyer et al.*, 2012] and a fluence of 1 photon/cm^2 was folded through the instrument response. The observed count fluence in each detector was taken as the effective area. These 10 estimates of the effective area were then averaged to arrive at a value of 161 ± 25 cm^2.

[35] The corrected fluence distribution in Figure 2 is shown as the number of TGFs per area and per unit time (TGFs km^{-2} h^{-1}) by accounting for the exposure time, the effective observational area, the sample size versus total TGFs observed, and the observational bias toward areas with a high rate of TGFs. The exposure time is the total duration of the TTE data collection in the 1 year time frame of the sample, or 939.6 h that includes all the triggered and nontriggered TGFs in our sample. The effective observational area can be calculated by integrating the rate density function that was fit to the GBM observed rate density versus nadir-source offsets [*Briggs et al.*, 2013, Figure 8b], obtaining an efficiency-weighted observing area for GBM of 6.85 × 10^5 km^2, or an effective observational radius of ∼467 km. The representative sample must be scaled up by a factor of 3.1

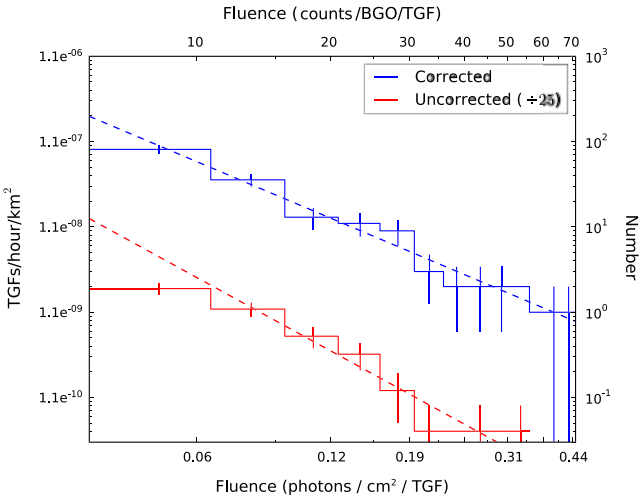

Figure 2. Power law fits to the corrected and uncorrected data where the uncorrected data are shifted downward by a factor of 25. A power law of index –2.20 ± 0.13 is best fit to the corrected data. The uncorrected data are fit with a power law of –2.86 ± 0.32.

to account for the fact that only 0.324 (triggered 12/37, untriggered 94/290) of the total TGFs that passed the probability cuts were selected for the sample. As data were only collected in the specific TTE boxes and not over the entire orbit of Fermi, a scaling factor of 4.2 [*Briggs et al.*, 2013] is applied to scale down the number of TGFs that would be observed over the entire orbit.

6. Discussion and Conclusions

[36] *Collier et al.* [2011] suggested that the observed fluence distribution of TGFs at satellite altitude can be described as a power law distribution. *Gjesteland et al.* [2011] showed that if a power law distribution is assumed, then the range of the index is $-1.9 > \alpha > -2.5$. Assuming a power law, *Østgaard et al.* [2012] estimated the power law index of –2.3 ± 0.2 for the observed fluence distribution using the relative sensitivities and observation rate of TGFs for Fermi GBM and RHESSI.

[37] In this work, individual TGFs are corrected for instrumental effects to determine the overall effect on the observed fluence distribution in GBM. As no model for the analysis was assumed a priori, different models can be fit to the data. A power law is the best fit model to the data in comparison to an exponential model. The fluence distribution obtained using corrected GBM data is best fit with a power law of index –2.20 ± 0.13. This result is consistent with the estimate obtained by *Østgaard et al.* [2012] and similarly corresponds to a true source distribution [*Carlson et al.*, 2012] of $\alpha \simeq -2.0 \pm 0.13$, assuming a single source altitude of 20 km.

[38] The magnitude of systematic uncertainties on the final result is challenging to quantify. *Byrne et al.* [2013] show that the dead-time deconvolution method is able to reconstruct the fluence of a simulated TGF and showed a 1:1 correspondence for a large sample of simulated TGFs. This shows that dead-time correction does not contribute to the systematic uncertainties. However, this method cannot be used for the detection efficiency as the true population of TGFs cannot be determined without a detection efficiency correction. Neglecting the lowest bin from the distribution (the only bin with a detection efficiency correction) yields a value of –2.40 ± 0.27 for the power law index. The value obtained for the entire corrected distribution is consistent with this value within the 1σ errors, implying that the statistical error dominates any systematic effect that may have been introduced by the detection efficiency correction.

[39] By integrating the area under the power law, a simple estimate of the TGF rate/yr can be calculated. If the limits of the integral are set to the 0% detection efficiency limit and the maximum of the data set (4.9 and 71 counts/BGO/TGF), a TGF rate of $(4.3 \pm 0.4) \times 10^5$ TGFs/yr between a latitude of ±25.6° is obtained. The uncertainty on the result is statistical only. If the *Briggs et al.* [2013] result is corrected to be at the same threshold as our work ($P_{\text{joint}}^{\text{corr}} < 10^{-16}$), a result of $(3.6 \pm 0.2) \times 10^5$ TGFs/yr is calculated. The TGF rate in *Briggs et al.* [2013] accounts for regional variations in the TGF/lightning ratio while that effect is not considered herein. This may not allow direct comparison between the results; however, our estimate is higher than the number modified from *Briggs et al.* [2013] which is likely due to correcting for detection efficiency.

[40] This work demonstrates that instrumental effects must be taken into consideration when performing analysis on TGFs. The fluence distribution is consistent with a power law over the entire range of TGF fluences in the sample.

[41] **Acknowledgments.** D.T. acknowledges support from Science Foundation Ireland under grant 09-RFP-AST-2400. G.F. acknowledges the support of the Irish Research Council. S.F. acknowledges the support of the Irish Research Council for Science, Engineering and Technology, cofunded by Marie Curie Actions under FP7. D.B. acknowledges support from the Programme for Research in Third Level Institutions (PRTLI) Cycle 5 and from the European Regional Development Fund. We thank the anonymous reviewers for helpful suggestions during the refereeing process.

[42] Robert Lysak thanks Nikolai Østgaard and an anonymous reviewer for their assistance in evaluating this paper.

References

Akaike, H. (1974), A new look at the statistical model identification, *IEEE Trans. Autom. Control*, *19*, 716–723.

Atwood, W. B., et al. (2009), The Large Area Telescope on the Fermi Gamma-ray Space Telescope mission, *Astrophys. J.*, *697*, 1071, doi:10.1088/0004-637X/697/2/1071.

Briggs, M. S., et al. (2010), First results on terrestrial gamma ray flashes from the Fermi Gamma-ray Burst Monitor, *J. Geophys. Res.*, *115*, A07323, doi:10.1029/2009JA015242.

Briggs, M. S., et al. (2013), Terrestrial gamma-ray flashes in the Fermi era: Improved observations and analysis methods, *J. Geophys. Res. Space Physics*, *118*, 3805–3830, doi:10.1002/jgra.50205.

Burnham, K. (2002), *Model Selection and Multimodel Inference: A Practical Information-Theoretic Approach*, Springer-Verlag, New York.

Byrne, D., M. S. Briggs, D. Tierney, G. Fitzpatrick, S. Foley, and S. McBreen (2013), A statistical dead-time deconvolution method for Fermi/GBM TGF observations, *EGU Gen. Assembly Conf. Abstr.*, *15*, 4331.

Carlson, B. E., T. Gjesteland, and N. Østgaard (2012), Connecting the terrestrial gamma-ray flash source strength and observed fluence distributions, *J. Geophys. Res.*, *117*, A01314, doi:10.1029/2011JA017122.

Celestin, S., and V. P. Pasko (2012), Compton scattering effects on the duration of terrestrial gamma-ray flashes, *Geophys. Res. Lett.*, *39*, L02802, doi:10.1029/2011GL050342.

Chaplin, V., N. Bhat, M. S. Briggs, and V. Connaughton (2013), Analytical modeling of pulse-pileup distortion using the true pulse shape; applications to Fermi-GBM, *Nucl. Instrum. Methods Phys. Res., Sect. A*, *717*, 21–36, doi:10.1016/j.nima.2013.03.067.

Collier, A. B., T. Gjesteland, and N. Østgaard (2011), Assessing the power law distribution of TGFs, *J. Geophys. Res.*, *116*, A10320, doi:10.1029/2011JA016612.

Dwyer, J. R., D. M. Smith, and S. A. Cummer (2012), High-energy atmospheric physics: Terrestrial gamma-ray flashes and related phenomena, *Space Sci. Rev.*, *173*, 133–196, doi:10.1007/s11214-012-9894-0.

Fishman, G. J., et al. (1994), Discovery of intense gamma-ray flashes of atmospheric origin, *Science*, *264*, 1313–1316, doi:10.1126/science.264.5163.1313.

Fishman, G. J., et al. (2011), Temporal properties of terrestrial gamma-ray flashes from the gamma-ray burst monitor on the Fermi observatory, *J. Geophys. Res.*, *116*, A07304, doi:10.1029/2010JA016084.

Gjesteland, T., N. Østgaard, P. H. Connell, J. Stadsnes, and G. J. Fishman (2010), Effects of dead time losses on terrestrial gamma ray flash measurements with the burst and transient source experiment, *J. Geophys. Res.*, *115*, A00E21, doi:10.1029/2009JA014578.

Gjesteland, T., N. Østgaard, A. B. Collier, B. E. Carlson, M. B. Cohen, and N. G. Lehtinen (2011), Confining the angular distribution of terrestrial gamma ray flash emission, *J. Geophys. Res.*, *116*, A11313, doi:10.1029/2011JA016716.

Gjesteland, T., N. Østgaard, A. B. Collier, B. E. Carlson1, C. Eyles, and D. M. Smith (2012), A new method reveals more TGFs in the RHESSI data, *Geophys. Res. Lett.*, *39*, L05102, doi:10.1029/2012GL050899.

Grefenstette, B. W., D. M. Smith, J. R. Dwyer, and G. J. Fishman (2008), Time evolution of terrestrial gamma ray flashes, *Geophys. Res. Lett.*, *35*, L06802, doi:10.1029/2007GL032922.

Grefenstette, B. W., D. M. Smith, B. J. Hazelton, and L. I. Lopez (2009), First RHESSI terrestrial gamma ray flash catalog, *J. Geophys. Res.*, *114*, A02314, doi:10.1029/2008JA013721.

Grove, J. E., A. Chekhtman, Fermi LAT Collaboration, G. Fishman, M. Briggs, V. Connaughton, and Fermi GBM Collaboration (2012), Observation of terrestrial gamma-ray flashes with Fermi LAT, *American Astronomical Society Meeting Abstracts*, *219*, 149.13.

Lewis, P. A. W., and G. S. Shedler, (1978), Simulation of nonhomogeneous poisson processes by thinning, *Tech. Rep. ADA059904*, Naval Postgraduate School, Naval Postgraduate School, Calif.

Marisaldi, M. (2011), *AGILE observations of terrestrial gamma-ray flashes*. http://arxiv.org/abs/1111.2188v1, eConf C110509.

Meegan, C. A., et al. (2009), The Fermi Gamma-ray Burst Monitor, *Astrophys. J.*, *702*, 791–804, doi:10.1088/0004-637X/702/1/791.

Nelder, J. A., and R. Mead (1965), A simplex method for function minimization, *Comput. J.*, *7*, 308–313.

Østgaard, N., T. Gjesteland, J. Stadsnes, P. H. Connell, and B. Carlson (2008), Production altitude and time delays of the terrestrial gamma flashes: Revisiting the burst and transient source experiment spectra, *J. Geophys. Res.*, *113*, A02307, doi:10.1029/2007JA012618.

Østgaard, N., R. Gjesteland, S. Hansen, A. B. Collier, and B. Carlson (2012), The true fluence distribution of terrestrial gamma flashes at satellite altitude, *J. Geophys. Res.*, *117*, A03327, doi:10.1029/2011JA017365.